How the Comet Crumbles: Mass Wasting Drives Outbursts on Comet 67P/Churyumov-Gerasimenko

Matthew R. Moser[1†], Abhinav S. Jindal[1*†], Jason M. Soderblom[2], Jean-Baptiste Vincent[3], Jordan K. Steckloff[4], Björn J. R. Davidsson[5], Eads Fouché[1], Raphael Marschall[6], Orkan M. Umurhan[7], Samuel P. D. Birch[1]

[1]Department of Earth, Environmental, and Planetary Sciences, Brown University, Providence, RI, USA.
[2]Department of Earth, Atmospheric and Planetary Sciences, Massachusetts Institute of Technology, Cambridge, MA, USA.
[3]Institute of Planetary Research, Deutsches Zentrum für Luft- und Raumfahrt, Berlin, Germany.
[4]Planetary Science Institute, Tucson, AZ, USA.
[5]Jet Propulsion Laboratory, California Institute of Technology, Pasadena, CA, USA.
[6]Centre National de la Recherche Scientifique, Laboratoire J.-L. Lagrange, Observatoire de la Côte d'Azur, Nice, France.
[7]SETI Institute at NASA Ames Research Center, Space Sciences Division, Moffett Field, CA, USA.

*Corresponding author(s). E-mail(s): abhinav_jindal@brown.edu;
†These authors contributed equally to this work.

Contents and organization

This Supplementary Information provides the complete observational record underlying the outburst–surface-change associations presented in the main text. It is organized into three parts. Section 1 presents a catalogue of all 37 regions of interest (ROIs), listing the associated outbursts, individual surface changes, change intervals, secondary plume observations, previously published changes, relative dust-plume luminosities (from Vincent et al. (2016)), and available CO_2/H_2O measurements (from Müller et al. (2024)). Section 2 details how we mapped the reconstructed outburst source footprints and ROI locations across the nucleus of 67P, providing the spatial context for the catalogue. Section 3 then documents the temporal evolution of each ROI individually, describing the available pre- and post-event imaging, the observed morphological changes, plume-source geometry, and the evidence used to associate each change with localized outburst activity.

For each ROI in which a morphological change is identified, we also provide supplementary videos documenting the available image sequences. These videos show the net surface modification and, where the imaging cadence permits, its temporal evolution. Where the data allowed, they videos also include the secondary plume observations and the catalogued outburst, each projected onto the nucleus, which allows the spatial relationship between plume activity and the changing surface to be examined directly.

Contents

1 Catalogue of outbursts and associated surface changes

Supplementary Table 1 provides the complete event-level catalogue used throughout this study. Because several outbursts originate from overlapping source regions, individual ROIs may contain multiple temporally distinct outbursts and multiple changed features. Where the available data permits, changes are associated with individual outbursts. Where it does not, the association is retained at the ROI level rather than assigning a change to a specific event.

Table 1: **Catalogue of outbursts and associated surface changes on 67P.** The table summarizes all 37 regions of interest (ROIs) examined in this study. Each ROI contains one or more reconstructed outburst source footprints and, where present, one or more changed surface features labelled 'a', 'b', 'c', etc. The "Change interval" brackets each morphological modification between the last suitable pre-change and first suitable post-change OSIRIS NAC observations. Change types are abbreviated as follows: CC-T, cliff collapse producing resolvable talus; CC-B, cliff collapse in which a coherent block remains largely intact; CC-N, cliff collapse leaving no resolvable debris; CC-U, cliff collapse for which the resulting debris cannot be determined; BD, boulder displacement; BF, boulder fragmentation; PF, pit formation or expansion; and SR, granular scarp retreat. "Secondary plumes" lists additional localized plume activity observed within the ROI outside the catalogued outburst itself. "Outburst ref." identifies the corresponding published or newly identified event, while "Prior change ref." denotes surface changes reported previously in the literature. "Rel. lum." gives the relative optical luminosity measured by Vincent et al. (2016), normalized to the brightest event in their catalogue (100%), and should be interpreted as a proxy for dust-plume brightness rather than ejected mass. The CO_2/H_2O column gives the peak enhancement of the CO_2/H_2O abundance ratio relative to the quiescent coma reported by Müller et al. (2024); "n.e." denotes no detected enhancement. A dash indicates that no corresponding measurement or constraint is available.

ROI	Outburst date(s)	Feature ID	Change interval	Change type	Secondary plumes	Outburst ref.	Prior change ref.	Rel. lum.[*]	CO_2/H_2O[†††]
1	2015-03-12	–	–	–	–	[†]	–	–	–
2	2015-07-10	–	2015-07-04–2015-07-15	CC-T	–	1[*]	[††]	–	–
3	2015-07-19, 2015-09-10	a	2015-05-02–2015-11-20	CC-T	2015-07-31, 2015-08-27	2[*], 27[*]	–	2.43, 6.47	8.3, n.e.
		b	2016-01-27–2016-06-09	CC-T	–				
		c	2015-05-02–2015-11-20	CC-T	2015-08-27				
		d	2015-05-02–2015-11-20	CC-T	–				
4	2015-07-26	a	2015-03-25–2016-02-10	CC-T	–	3[*]	–	7.07	19.7
		b	2015-03-25–2016-02-10	BD	–				
		c	2015-03-25–2016-02-10	BF	2015-08-27, 2015-10-31				
		d	2015-03-25–2016-02-10	BD	–				
		e	2015-03-25–2016-02-10	CC-T	–				
		f	2015-03-25–2016-02-10	CC-U	–				
5	2015-07-27, 2015-09-05	a	2015-05-02–2016-01-27	CC-T	–	4[*], 25[*]	–	1.94, 66.73	21.8, —

Continued on next page

Table 1 (Continued)

ROI	Outburst date(s)	Feature ID	Change interval	Change type	Secondary plumes	Outburst ref.	Prior change ref.	Rel. lum.*	CO_2/ H_2O†††
6	2015-07-28	a	2015-04-25–2015-07-25	SR	–	5*	‡‡ (Fig. S10)[a]	0.51	6.9
7	2015-08-09	a	2015-05-02–2015-11-20	BD	–	13*	–	3.05	6.9
		b	2015-05-02–2015-11-20	CC-T	–				
	2015-07-29	c	2015-05-02–2015-11-20	BD	–	6*	–	15.58	18.8
8	2015-08-01	a	2015-08-01 08:02–20:56	CC-B	2015-08-01[b]	7*, 33*[c]	#	1.41	13.8
	2015-09-14	b	2015-05-23–2015-10-29	SR	2015-07-30, 2015-07-31		#	35.21	0.9
	2015-09-14	c	2015-05-23–2015-10-29	CC-N	2015-08-01		–		
	–	d	2015-12-10–2016-01-23	BD	2015-12-10		##, #		
9	2015-08-01	–	2015-04-13–2016-02-10	BD[d]	2015-08-01[d]	8*	–	11.71	16.1
10	2015-08-03	–	2015-05-02–2016-01-27	PF	–	9*	–	0.55	2.2
11	2015-08-05, 2015-08-22	a	2015-05-02–2016-01-27	BD	–	10*, 17*	–	1.90, 0.29	23.9, 18.7
	2015-08-05, 2015-08-22	b		CC-B		10*, 17*			
	2015-08-05	c		–		11*		1.90	23.9
	2015-08-23	d		BD[e]		19*		5.46	18.7
12	2015-08-06	–	2015-05-22–2015-12-10	SR	–	N1	–	–	–
13	2015-08-08	a	2015-05-02–2015-10-29	CC-B	–	12*	–	–	14.0
14	2015-08-10	a	2015-05-02–2016-01-27	BD	–	§	–	–	–
15	2015-08-12	a	2015-05-02–2015-11-19	SR	2015-06-05, 2015-12-07[f]	14*	¶¶ (Fig. 3)	100	0.6
		b	2015-05-02–2015-11-19	SR	–		¶¶ (Fig. 7)		
		c	2015-11-19–2016-01-27	SR	–		¶¶ (Fig. 7)		
		d	2015-05-02–2015-11-19	BF	–		¶¶ (Fig. 7)		
16	2015-08-21	a	2015-03-10–2015-11-28	BD	2015-06-27	15*	–	–	4.1
		b	2015-03-10–2015-11-28	BD	–		–		
		c	2015-11-28–2015-12-07	CC-B	–		–		
17	2015-08-22	a	2015-08-01–2015-10-29	CC-N	–	16*	–	–	24.3

Continued on next page

Table 1 (Continued)

ROI	Outburst date(s)	Feature ID	Change interval	Change type	Secondary plumes	Outburst ref.	Prior change ref.	Rel. lum.[*]	CO_2/ H_2O[†††]
18	2015-08-23	a	2015-05-24– 2015-10-29	BD	–	18[*]	–	12.53	4.3
		b	2015-05-24– 2016-01-30	BF					
		c	2015-05-24– 2016-01-30	BF					
19	2015-08-26	–	–	–	–	20[*]	–	5.57	15.1
20	2015-08-27	a	2015-03-20– 2015-12-26	SR	–	21[*]	–	2.71	18.7
		b	2015-03-20– 2015-12-26	BD					
21	2015-08-28, 2015-09-05	a	2015-05-02– 2016-01-27	CC-U	–	22[*], 24[*]	–	29.04, 27.89	5.1, —
22	2015-08-28	–	2015-05-02– 2016-02-07	PF	–	23[*]	–	69.84	4.1
23	2015-09-10	a	2015-05-02– 2015-10-29	BF	–	26[*]	–	1.83	n.e.
24	2015-09-10	a	2015-03-20– 2016-06-09	CC-T	–	28[*]	–	9.44	n.e.
		b	2015-03-20– 2016-06-09	BF	–				
25	2015-09-10	a	2015-05-02– 2015-10-31	CC-B	–	29[*]	–	7.97	n.e.
26	2015-09-10	a	2015-05-02– 2016-01-27	CC-U	–	30[*]	–	4.37	n.e.
27	2015-09-10	a	2015-05-02– 2015-11-20	CC-T	–	31[*]	–	7.45	n.e.
		b	2015-05-02– 2015-11-20	BD					
28	2015-09-12	a	2015-05-24– 2015-12-10	CC-T	–	32[*]	[§§] (Fig. 2)[g]	15.96	1.0
29	2015-09-13	a	2015-08-24– 2015-10-28[h]	BD	2015-11-02	[‡], [§]	[‡‡] (Fig. S4), [#] (Fig. 3)	–	–
		b	2015-05-02– 2016-02-07	CC-N	2016-01-01		–		
		c	2015-05-02– 2016-02-07	CC-N	2016-01-01		–		
		d	2015-05-02– 2016-01-02	SR	–		[##] (Fig. 4)		
		e	2015-05-02– 2016-01-02	SR	–		–		
30	2015-09-26	a	2015-05-09– 2016-02-13	CC-T	–	34[*]	–	–	–
		b	2015-05-09– 2016-02-13	BD	–		–		
31	2015-11-22	a	2015-05-02– 2015-11-22	CC-T	–	N2, N3	–	–	–
	2015-10-29	b	2015-05-02– 2016-01-27	CC-T	–		–		

Continued on next page

Table 1 (Continued)

ROI	Outburst date(s)	Feature ID	Change interval	Change type	Secondary plumes	Outburst ref.	Prior change ref.	Rel. lum.[*]	CO_2/ H_2O[†††]
32	2015-10-30	a	2015-04-12–2015-10-30	BD	–	N4	–	–	–
	2015-10-30	b	2015-04-12–2016-02-10	SR	–	N4			
	2015-12-09	c	2015-04-12–2016-02-10	BD	–	N5			
33	2015-11-07	a	2015-05-02–2016-01-27	CC-T	–	A[¶]	–	–	–
		b	2015-05-02–2016-01-27	BD	–		–		
34	2015-11-07	–	–	–	–	B[¶]	–	–	–
35	2015-11-22	a	2015-05-02–2016-01-27	SR	–	N6	–	–	–
36	2015-12-13	a	2015-05-02–2016-02-07	CC-N	2016-01-01	E35[#]	–	–	–
37	2016-07-03	a	2016-05-02–2016-07-09	SR	–	[**]	–	–	–

References: [*]Vincent et al. (2016); [†]Knollenberg et al. (2016); [‡]Bockelée-Morvan et al. (2017); [§]Rinaldi et al. (2018); [¶]Noonan et al. (2021); [#]Hasselmann et al. (2019); [**]Agarwal et al. (2017); [††]Pajola et al. (2017); [‡‡]El-Maarry et al. (2017); [§§]El-Maarry and Driver (2019); [¶¶]Fornasier et al. (2019); [##]Deshapriya et al. (2016); [†††]Müller et al. (2024); [‡‡‡]Fornasier et al. (2017); [§§§]Tang et al. (2025).

Notes: [a]Change reported by El-Maarry et al. (2017) but not linked to an outburst; the change initiates before the outburst. [b]Numerous plumes on 2015-08-01 documented by Hasselmann et al. (2019). [c]Outburst 33 of Vincent et al. (2016) is the 2015-09-14 outburst of Bockelée-Morvan et al. (2017) and Rinaldi et al. (2018). [d]Displaced boulder lies adjacent to, not within, the outburst source; the 2015-08-01 plume is seen slightly above the boulder. Possibly a by-product of seismic disturbance rather than a direct outburst effect. [e]Displacement likely sourced from upslope, or boulder exposure. [f]Secondary plumes shown in Fig. 12 of Fornasier et al. (2017)[‡‡‡]. [g]Collapse captured by El-Maarry and Driver (2019); timing narrowed here. [h]Tang et al. (2025)[§§§] constrain the displacement to 2015-10-03.

2 Outburst source footprints and ROI locations

Supplementary Figure 1 shows the spatial distribution of the outbursts and surface-change regions summarized in Table 1. We display the nucleus of 67P from six orthogonal viewing directions so that source regions distributed across both lobes and both hemispheres can be seen without severe projection distortion. Outburst footprints represent the reconstructed surface locations of the observed plumes, whereas the larger ROI boundaries delimit the regions that we searched over for associated morphological change. Because multiple outburst footprints can overlap spatially, several individual events may fall within the same ROI. The outburst footprints associated with ROI 29 (Rinaldi et al. 2018) and ROIs 33 and 34 (Noonan et al. 2021) are not shown because their reported source regions are substantially larger than those of the other events and would obscure much of the surrounding surface in this visualization. These events are nevertheless included in the full ROI analysis and catalogue.

The tools that we used to (1) determine these locations, (2) find and map project all images locally, and (3) make of our all quantitative analyses are archived on Zenodo (detailed in the 'Data Availability' and 'Code Availability' sections of the main paper). We encourage the reader to make use of the tools, and/or reach out to the corresponding author, as we found that viewing the data natively in these tools is always preferred over looking at outputted images or videos.

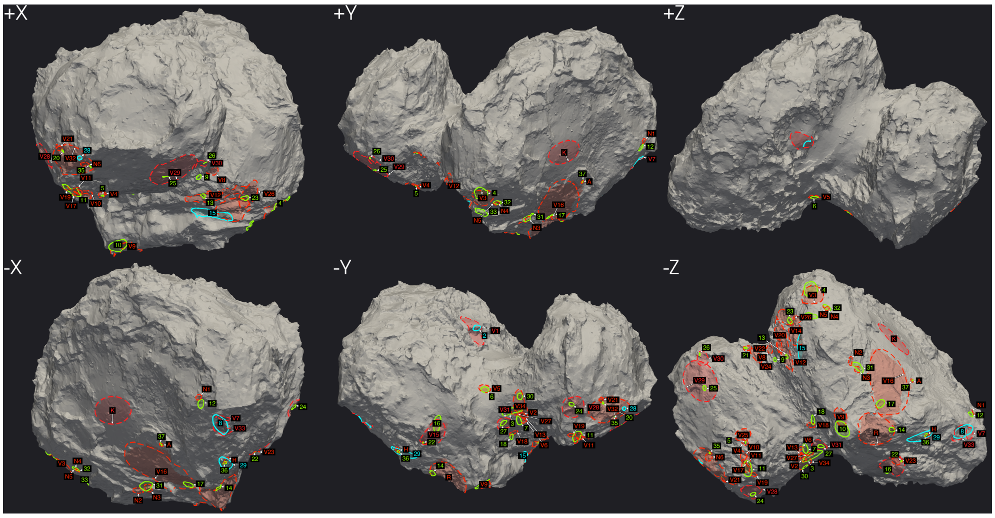

Fig. 1 Outburst source footprints and associated surface-change regions on comet 67P. The SHAP7 shape model of 67P (Preusker et al. 2017) is shown in orthographic projection along the six body-fixed directions ($\pm X$, $\pm Y$, $\pm Z$). Red dashed outlines mark the reconstructed source footprints of localized outbursts for which a surface location can be determined. Labels V1–V34 correspond to the outbursts catalogued by Vincent et al. (2016); K denotes the March 12, 2015 event of Knollenberg et al. (2016); R the August 10, 2015 event of Rinaldi et al. (2018); H event 35 of Hasselmann et al. (2019); A the July 3, 2016 event of Agarwal et al. (2017); and N1–N6 the six previously unreported outbursts identified in this study. Solid outlines mark the ROIs in which associated morphological changes are identified. Cyan outlines denote ROIs containing surface changes previously linked to outburst activity, whereas green outlines denote outburst-associated changes identified here for the first time. Multiple outburst footprints may occur within a single ROI where their reconstructed source regions overlap or lie sufficiently close that their surface evolution is best analysed together.

3 ROI-by-ROI surface evolution

The following subsections provide the complete observational history for each ROI, including the associated outburst(s), the timing and morphology of any detected surface changes, secondary plume activity where available, and the evidence used to link individual changes to localized activity. Where multiple outbursts or changed features occur within the same ROI, we distinguish individual associations when the imaging geometry and temporal coverage permit; otherwise, the relationship is retained at the ROI level.

For each ROI in which a morphological change is identified, the corresponding supplementary videos provide the visual record of this evolution, including the net pre- to post-change comparison and, where available, the intermediate temporal sequence, secondary plume observations, and the catalogued outburst projected onto the surface. We therefore encourage readers to view the videos alongside the ROI descriptions below.

3.1 ROI 1

ROI 1 corresponds to the small nightside outburst observed on March 12, 2015 by Knollenberg et al. (2016). The event had an average dust production rate of only $\sim$ 1 kg s^{-1} during its initial few minutes (Knollenberg et al. 2016), compared with $\sim$ 60–260 kg s^{-1}. Compared to the perihelion outburst in the Vincent et al. (2016) catalogue, this is small. Using our refined projection tool, we place the outburst footprint directly on the central scarp in Imhotep. No resolvable morphological change is observed at this location following the outburst, and the scarp remains unchanged until at least June 3, 2015 Jindal et al. (2022). We therefore cannot confidently associate this event with a visible surface modification. Given the small magnitude of the outburst, a localized disturbance below the spatial resolution of the available OSIRIS images cannot be excluded.

3.2 ROI 2

ROI 2 corresponds to the Aswan cliff collapse linked to an outburst on July 10, 2015 (outburst #1 in Vincent et al. (2016)), which was examined in detail by Pajola et al. (2017). This event was thoroughly documented, and we do not find any additional changes to report here. We include ROI 2 in our catalogue as a previously established case of outburst-associated cliff collapse and use it as a reference point for comparison with newly identified collapse events elsewhere on the nucleus.

3.3 ROI 3

ROI 3 contains one of the clearest examples of cascading cliff collapse identified in this study. We observe retreat at four distinct locations along the cliff boundary, labelled 'a', 'b', 'c', and 'd'. Comparison between images acquired on May 2, 2015 and June 9, 2016 shows that all four locations retreated during this interval, locally by more than 50 m. Intermediate imaging reveals that the collapse did not occur as a single catastrophic event: locations 'a', 'c', and 'd' had already failed by November 20, 2015, whereas location 'b' remained largely intact until at least January 27, 2015.

This region spans the estimated footprints of two outbursts reported by Vincent et al. (2016): outburst #2 on July 19, 2015 and outburst #27 on September 10, 2015. In both cases, the reported source region was beyond the local horizon at the time of observation, preventing the main outburst plumes from being traced directly onto the visible surface. Nevertheless, the reconstructed footprints fall in the vicinity of the collapsing cliff.

Additional plume observations strengthen this association. Smaller-scale plume activity is observed from cliff segment 'a' on July 31 and August 27, 2015, and from the base of segment 'c' on August 27, 2015. These plume sources coincide exactly with portions of the cliff underwent substantial retreat. We therefore classify ROI 3 as an outburst-associated cascading cliff collapse, in which repeated localized activity and sequential mass wasting reshaped multiple segments of the same cliff over a period of months.

3.4 ROI 4

ROI 4 is associated with the estimated location of outburst #3 of Vincent et al. (2016), observed on July 26, 2015, and contains multiple surface changes within the reported source region. We divide the observed modification into six features, labelled 'a'–'f'. All changes occurred between March 25, 2015 and February 10, 2016; the available images acquired between these dates do not provide sufficient spatial resolution or illumination to constrain the timing more precisely.

The changes in this region involve mass wasting of consolidated material. At features 'a' and 'e', cliffs retreat and leave talus deposits at their bases. Feature 'f' may represent an additional instance of cliff retreat, although much of this area is covered in shadow and the change cannot be confirmed with the same confidence. At features 'b' and 'd', two large boulders are displaced, indicating localized disturbance of the surface. Finally, feature 'c' involves the disappearance of two large boulders, suggesting that they may have crumbled into material too fine to resolve in the available images (the material may also be lost if it became too fine).

Plume activity is observed in the vicinity of feature 'c' on August 27 and October 31, 2015, linking these changes to repeated localized activity within the outburst source region.

3.5 ROI 5

ROI 5 overlaps with the estimated footprints of two outbursts reported by Vincent et al. (2016): outburst #4 on July 27, 2015 and outburst #25 on September 5, 2015. The reported sources lie within a large pit whose base remains shadowed or poorly resolved in the available images throughout most of the mission, limiting our ability to assess modification on the pit floor.

Nevertheless, we identify one surface change along the pit margin at feature 'a'. Between May 2, 2015 and January 27, 2016, a small cliff collapses and leaves talus at its base.

3.6 ROI 6

ROI 6 corresponds to the estimated footprint of outburst #5 of Vincent et al. (2016), observed on July 28, 2015. This region provides a clear example in which surface modification begins before the detected outburst. Two episodes of scarp retreat are observed in the reported source region during the months preceding the event.

The first episode occurs between April 25 and May 22, 2015, when eastward-migrating scarps remove a layer of smooth terrain. A second phase begins later in the apparition: from June 27 to July 25, 2015, the modified area expands more broadly, with scarp retreat occurring along multiple margins of the deposit rather than in a single preferred direction. The outburst is observed only a few days later, on July 28, 2015, from the same ROI. These surface changes were also reported by El-Maarry et al. (2017), although they were not linked to the July 28 outburst.

We therefore interpret ROI 6 as a case in which erosion of smooth terrain likely exposed underlying volatile-rich material before the observed outburst. Rather than representing only the aftermath of explosive activity, the scarp retreat in this region appears to mark a preparatory stage in which progressive removal of surface material enabled later volatile-driven activity.

3.7 ROI 7

ROI 7 spans three outburst footprints reported by Vincent et al. (2016): outburst #6 on July 29, outburst #13 on August 9, and outburst #34 on September 26, 2015. We identify three surface changes in this region, all occurring between May 2, 2015 and November 20, 2015. At feature 'a', a large boulder is displaced across the surface. At feature 'b', a cliff retreats and leaves a debris deposit at its base. At feature 'c', another boulder is displaced along the edge of a cliff, suggesting localized crumbling of the cliff margin.

The three outbursts cannot all be assigned to individual features. Outbursts #13 and #34 originated beyond the local horizon in the available images, preventing them from being traced directly onto the visible surface. However, outburst #6 originates at feature 'c' exactly, providing a direct link between observed changes and outburst activity.

3.8 ROI 8

ROI 8 is associated with two outbursts reported by Vincent et al. (2016): outburst #7 on August 1, 2015 and outburst #33 on September 14, 2015. This region contains several distinct surface changes involving both consolidated cliffs and smooth granular deposits. We divide the observed modification into four features, labelled 'a'–'d'.

Feature 'a' provides one of the strongest direct links between outburst activity and structural failure in our survey. A large consolidated block detached from the cliff within hours of outburst #7, at the same exact location from which the main plume was observed to emerge. The available image cadence does not allow us to determine whether the collapse triggered the outburst or whether the outburst caused the collapse. However, smaller plumes continued to emerge from the collapsed region for several hours after the main event, indicating that activity persisted at the failure site, possibly due to the block's detachment exposing deeper ices.

Feature 'b' records retreat of a granular scarp within the adjacent smooth deposit. Between May 23 and October 29, 2015, the scarp migrated across the deposit, leaving several larger embedded boulders exposed on the newly revealed surface. Smaller plumes are observed from this location beginning a few days before outburst #7, on July 30, 2015, and continuing until December 10, 2015. These plumes track the retreating scarp front, indicating that activity migrated with the evolving surface. Continued retreat eventually left a boulder perched at the scarp edge, labelled 'd', which fell on January 23, 2016 and exposed volatile-rich material (bright patch 2 in Deshapriya et al. (2016)). We therefore interpret feature 'd' as a consequence of the scarp retreat at feature 'b', rather than an independent outburst source.

These changes and associated plume observations were also reported by Hasselmann et al. (2019). However, our analysis identifies an additional change at feature ‘c’, where a large portion of a cliff retreated between May 23 and October 29, 2015, leaving no resolvable debris deposit behind. A small plume is observed near this location on August 1, 2015. We also disagree with their interpretations of feature ‘a’: we favour the simpler explanation that a block detached from the cliff and toppled over due to gravity, rather than this block getting delivered to the base of the cliff ballistically from a different region of the nucleus.

Outburst #33 also falls within ROI 8, but its source was beyond the local horizon when observed, preventing it from being traced directly onto the visible surface. It may therefore be associated with either the retreating scarp at feature ‘b’ or the cliff retreat at feature ‘c’, although the available viewing geometry prevents a unique assignment.

3.9 ROI 9

ROI 9 spans the estimated footprint of outburst #8 of Vincent et al. (2016), observed on August 1, 2015. The outburst plume is clearly visible within the ROI, providing a direct association between the reported activity and this localized region. However, the immediate source area is affected by shadowing and limited spatial resolution, preventing us from determining whether the surface directly beneath the plume underwent resolvable morphological change.

The only visible disturbance occurs just outside the apparent outburst source region. A large boulder, labelled ‘a’, located downslope of the plume source, was displaced between June 4, 2015 and February 10, 2016. Although this change cannot be assigned directly to the outburst footprint, its proximity to the source region suggests that the surrounding surface was disturbed during the same broad episode of localized activity. Within the outburst source itself, no resolvable surface change can be confirmed from the available data.

3.10 ROI 10

ROI 10 spans the estimated footprint of outburst #9 of Vincent et al. (2016). The region consists of heavily fractured consolidated terrain and several already-existing pits. Between May 2, 2015 and January 27, 2016, we observe both the formation of new pits and the expansion of several of the existing pits within the outburst footprint.

No plume activity is observed within this ROI in the available images. We therefore classify ROI 10 as an outburst-associated pit-formation and pit-expansion site, although the available observations do not allow the timing of individual pit changes to be constrained more precisely.

3.11 ROI 11

ROI 11 spans a cluster of four outburst footprints reported by Vincent et al. (2016): outbursts #10 and #11 on August 5, 2015, outburst #17 on August 22, 2015, and outburst #19 on August 23, 2015. We identify four surface changes in this region, labelled ‘a’–‘d’, all occurring between May 2, 2015 and January 27, 2016. The available images acquired between these dates do not provide sufficient spatial resolution or illumination to constrain the timing more precisely.

At feature ‘a’, a boulder moves downslope, while at feature ‘b’, a single consolidated block detaches from the edge of a cliff. These two changes lie within the portion of the ROI associated with outbursts #10 and #17, but the available observations do not allow either change to be assigned uniquely to one of the two events. Feature ‘c’ lies within the estimated footprint of outburst #11. This area is largely covered in shadow in the earlier images, making it difficult to determine whether a resolvable surface change occurred there. Finally, feature ‘d’ lies within the estimated footprint of outburst #19, where a new boulder appears on the surface, likely derived from crumbling of the cliff farther upslope.

3.12 ROI 12

ROI 12 corresponds to a previously unreported outburst that we identified in our study here. It occurred on August 6, 2015 and is located in the vicinity of ROI 8. The region shows terraced scarp retreat within a smooth granular deposit, strikingly similar to feature ‘b’ in ROI 8. Between May 22 and December 10, 2015, the scarp migrated across the deposit, exposing the underlying surface and leaving embedded boulders behind.

3.13 ROI 13

ROI 13 spans the estimated footprint of outburst #12 of Vincent et al. (2016), observed on August 8, 2015. At feature ‘a’, we observe a cliff collapse between May 2 and October 29, 2015, in which a single consolidated block detached from the cliff and remained largely intact after falling.

3.14 ROI 14

ROI 13 sits within the estimated footprint of the August 10, 2015 outburst reported by Rinaldi et al. (2018). Within this region, we observe a large boulder (feature ‘a’) migrate downslope between May 2, 2015 and January 27, 2016.

3.15 ROI 15

ROI 15 is associated with outburst #14 of Vincent et al. (2016), observed on August 12, 2015. This region contains four distinct surface changes, labelled ‘a’–‘d’. Features ‘a’, ‘b’, and ‘d’ occurred between May 2 and November 19, 2015, whereas feature ‘c’ occurred later, between November 19, 2015 and January 27, 2016.

At feature ‘a’, a terraced scarp retreats within a smooth deposit, displacing a large boulder that was initially perched on top of the scarp. Smaller plumes are also observed from this region on June 5 and December 7, 2015, indicating repeated localized activity. At feature ‘b’, a similar terraced scarp retreat results in the disintegration of a large boulder mound initially embedded along the scarp edge. At feature ‘d’, a single boulder breaks apart into at least three pieces. Finally, at feature ‘c’, we observe another terraced scarp retreat leaving embedded boulders at its base. All these changes were first attributed to the same outburst by Fornasier et al. (2019).

3.16 ROI 16

ROI 16 spans the estimated footprint of outburst #15 of Vincent et al. (2016), observed on August 21, 2015. We identify three large-scale changes within this region. Between March 10 and November 28, 2015, new talus appears at feature 'a', likely sourced from a cliff farther upslope where plume activity is observed on June 27, 2015. Over the same interval, a large boulder at feature 'b' detaches from its consolidated substrate. A later change occurs at feature 'c', where a cliff collapses between November 28 and December 7, 2015. Unlike the talus-forming collapse at feature 'a', this failure produced a single large consolidated block that detached from the cliff and remained largely intact after falling.

The estimated footprint of outburst #15 is broad, making it difficult to determine which individual feature corresponds directly to the August 21 event. However, the timing of feature 'c' indicates that this collapse occurred months after the main outburst and therefore likely reflects secondary activity within the same localized region.

3.17 ROI 17

ROI 17 spans the estimated footprint of outburst #16 of Vincent et al. (2016), observed on August 22, 2015. We identify one notable change in this region: a cliff collapse at feature 'a' between August 1 and October 29, 2015. No resolvable debris deposit is left behind, suggesting that the collapsed material either fragmented into particles below the available image resolution or was dispersed from the immediate source region.

3.18 ROI 18

ROI 18 spans the estimated footprint of outburst #18 of Vincent et al. (2016), observed on August 23, 2015. We identify three changes within the same region. At feature 'a', a boulder detaches from its substrate and moves downslope between May 24 and October 29, 2015. At features 'b' and 'c', two additional boulders disintegrate into smaller fragments between May 24, 2015 and January 30, 2016.

3.19 ROI 19

ROI 19 spans the estimated footprint of outburst #20 of Vincent et al. (2016), observed on August 26, 2015. The source region lies within the rugged topography of the southern hemisphere and remained heavily shadowed until later in the mission. As a result, no suitable pre-outburst observations of the surface are available, preventing us from assessing whether any resolvable morphological change accompanied the event.

3.20 ROI 20

ROI 20 covers a large pit from which outburst #21 of Vincent et al. (2016) originated on August 27, 2015. Within this pit, we identify two surface changes between March

20 and December 26, 2015. At feature ‘a’, a terraced scarp retreats across the pit floor. At feature ‘b’, a new boulder appears on the surface, likely produced by crumbling of the pit margin.

3.21 ROI 21

ROI 21 spans the overlapping footprints of outburst #22 on August 28, 2015 and outburst #24 on September 5, 2015, both reported by Vincent et al. (2016). The region consists of rugged consolidated terrain, and the available images provide only limited views of the candidate source area. We identify a possible cliff retreat at feature ‘a’ between May 2, 2015 and January 27, 2016, but the complex topography and changing illumination make this change difficult to confirm. The base of the cliff is also covered in shadow in the available post-collapse images, so we cannot determine whether any resolvable debris was produced.

3.22 ROI 22

ROI 22 spans the estimated footprint of outburst #23 of Vincent et al. (2016), observed on August 28, 2015. The region consists of heavily fractured consolidated terrain containing a pre-existing pit. Between May 2, 2015 and February 7, 2016, we see this pit expand into the surrounding terrain at feature ‘a’.

3.23 ROI 23

ROI 23 overlaps with the estimated footprint of outburst #26 of Vincent et al. (2016), observed on September 10, 2015. Within this region, a large boulder at feature ‘a’ disintegrates into smaller fragments between May 2 and October 29, 2015.

3.24 ROI 24

ROI 24 overlaps with the estimated footprint of outburst #28 of Vincent et al. (2016), observed on September 10, 2015. We identify a large cliff collapse within this region between March 20, 2015 and June 9, 2016. No suitable intermediate images are available to constrain the timing more precisely.

The collapse occurred on the far side of the cliff relative to the available viewing geometries, so the failure surface is only partially visible in the post-collapse images. Some debris can be seen near the base of the cliff, but the viewing geometry prevents us from estimating the full extent of the deposit.

3.25 ROI 25

ROI 25 overlaps with the estimated footprint of outburst #29 of Vincent et al. (2016), observed on September 10, 2015. We identify a cliff collapse at feature ‘a’ between May 2 and October 31, 2015, in which a single consolidated block detached from the cliff and remained largely intact after falling.

3.26 ROI 26

ROI 26 overlaps with the estimated footprint of outburst #30 of Vincent et al. (2016), observed on September 10, 2015. At feature 'a', we observe a cliff collapse May 2, 2015 and January 27, 2016. The nature of the debris is difficult to verify since the region is covered in shadow pre-collapse.

3.27 ROI 27

ROI 27 overlaps with the estimated footprint of outburst #31 of Vincent et al. (2016), observed on September 10, 2015. Between May 2 and November 20, 2015, we identify two changes within the source region. At feature 'a', a cliff retreats and leaves a debris deposit at its base. At feature 'b', a large boulder in the immediate vicinity of the cliff detaches and moves downslope.

3.28 ROI 28

ROI 28 is associated with outburst #32 of Vincent et al. (2016), observed on September 12, 2015. This region underwent a large-scale cliff collapse between May 24 and December 10, 2015, producing a substantial talus deposit at the base of the cliff. This outburst induced collapse was first reported by El-Maarry and Driver (2019).

3.29 ROI 29

ROI 29 spans the estimated footprint of the September 13, 2015 outburst reported by Bockelée-Morvan et al. (2017) and Rinaldi et al. (2018). We identify five surface changes within this region, labelled 'a'–'e'.

At feature 'a', a large ∼30 m boulder moves downslope (El-Maarry et al. 2017). This displacement was previously linked either directly to an outburst or to seismic disturbance from a nearby active source (Hasselmann et al. 2019). However, more recent work precisely timed the motion to October 3, 2015 and suggested that it may instead have been driven by outgassing from beneath the boulder itself (Tang et al. 2025). We therefore include feature 'a' as evidence for substantial activity-related disturbance within ROI 29, but caution that its connection to the September 13 outburst remains uncertain.

At features 'b' and 'c', portions of the cliff disappear between May 2, 2015 and February 7, 2016, leaving no resolvable debris behind. At features 'd' and 'e', terraced scarps retreat between May 2, 2015 and January 2, 2016, exposing spectrally blue, volatile-rich subsurface material (Deshapriya et al. 2016). At feature 'd', we also observe a boulder at the scarp edge disintegrate during this interval.

Additional plume activity is observed near feature 'a' on November 2, 2015, and near features 'b' and 'c' around January 1, 2016. These observations indicate repeated localized activity across ROI 29, although the available data do not allow all individual surface changes to be uniquely assigned to the September 13 outburst.

3.30 ROI 30

ROI 30 overlaps with the estimated footprint of outburst #34 of Vincent et al. (2016), observed on September 26, 2015. We identify two major changes within this region, both occurring between May 9, 2015 and February 13, 2016. At feature ‘a’, a cliff retreats from two directions and leaves debris accumulated at its base. At feature ‘b’, a boulder is displaced across the surface.

3.31 ROI 31

ROI 31 is associated with two previously unreported outbursts that we have identified in this study, one observed on October 29 and the other November 22, 2015. Both outbursts emerge from the same connected cliff face, but from different locations along it. We identify two corresponding cliff-collapse features, labelled ‘a’ and ‘b’.

Feature ‘a’ is associated with the November 22 outburst. Between May 2 and November 23, 2015, part of the cliff collapsed, producing newly exposed debris and large boulders at its base.

Feature ‘b’ is associated with the October 29 outburst and records a similar collapse along another part of the same cliff face between May 2, 2015 and January 27, 2016.

3.32 ROI 32

ROI 32 contains another two previously unreported outbursts that we identified in this study, one on October 30 and December 9, 2015. This region provides another clear example in which surface modification *preceded* the observed outburst. Before activity was detected, the region contained a terraced granular scarp, labelled ‘b’, with a large boulder, labelled ‘a’, perched on the upper part of the deposit. Between April 12 and October 30, 2015, boulder ‘a’ moved downslope from the top of the scarp. Although the scarp itself is not sufficiently visible in the October 30 image to determine its exact state at that time, it had fully disappeared by February 10, 2016.

The October 30 outburst then emerges from the exact initial location of boulder ‘a’, after the boulder had already moved to its final position. This timing indicates that surface unloading occurred before the detected outburst. We interpret the sequence as progressive retreat of the granular scarp ‘b’, driven by daily activity or smaller unobserved plumes, eventually destabilizing boulder ‘a’ and allowing it to roll downslope. Removal of the boulder and surrounding sediment then exposed deeper volatile-rich material. Now suddenly closer to the surface, this would dramatically increasing outgassing rates, manifesting as the October 30 outburst.

A second, smaller plume is observed in the region on December 9, 2015. This later activity is associated with displacement of another boulder, labelled ‘c’, indicating that localized disturbance continued after the initial outburst.

3.33 ROI 33

ROI 33 overlaps with the estimated footprint of outburst A reported by Noonan et al. (2021), observed on November 11, 2015. We identify two major surface changes within this ROI, both occurring between May 2, 2015 and January 27, 2016. At feature ‘a’, a cliff collapses and leaves a debris deposit at its base. At feature ‘b’, a nearby boulder is displaced across the surface.

3.34 ROI 34

ROI 34 corresponds to outburst B of Noonan et al. (2021), observed on November 7, 2015. The reported source footprint for this event spans a very large area of the nucleus, preventing any meaningful localized search for associated morphological change. We therefore do not assess surface modification for this event and classify ROI 34 as having insufficient spatial constraint for change analysis.

3.35 ROI 35

ROI 35 is associated with another previously unreported outburst we identified now in this study. It occurred on November 22, 2015. Within this region, we observe terraced scarp retreat in a smooth granular deposit at feature ‘a’. Between May 2, 2015 and January 27, 2016, the scarp migrated across the deposit, exposing the underlying surface and leaving large embedded boulders behind.

3.36 ROI 36

ROI 36 corresponds to the December 13, 2015 outburst reported as event 35 by Hasselmann et al. (2019). At feature ‘a’, which overlaps with the outburst source region, portions of a cliff disappear between May 2, 2015 and February 7, 2016, leaving no resolvable debris behind.

3.37 ROI 37

ROI 37 corresponds to the July 3, 2016 outburst reported by Agarwal et al. (2017). This event was previously associated with the exposure of bright material on the surface between May 2 and July 9, 2016. Agarwal et al. (2017) suggested two possible interpretations for this exposure: either a sharply bounded coating of ice on the bouldered surface, or freshly excavated subsurface material exposed along a topographic edge.

Our analysis favours the latter interpretation. The bright exposure, labelled ‘a’, occurs along the retreating edge of a granular scarp, indicating that it represents freshly exposed subsurface material rather than a surface coating. This interpretation is supported by the disappearance of two boulders perched on the scarp edge, labelled ‘b’ and ‘c’, which likely fell into the shadowed base of the scarp as the scarp retreated.

References

Agarwal J, Della Corte V, Feldman PD, et al (2017) Evidence of sub-surface energy storage in comet 67P from the outburst of 2016 July 03. Monthly Notices of the Royal Astronomical Society 469(Suppl_2):s606–s625. https://doi.org/10.1093/mnras/stx2386

Bockelée-Morvan D, Rinaldi G, Erard S, et al (2017) Comet 67P outbursts and quiescent coma at 1.3 au from the Sun: dust properties from Rosetta/VIRTIS-H observations. Monthly Notices of the Royal Astronomical Society 469(Suppl_2):S443–S458. https://doi.org/10.1093/mnras/stx1950

Deshapriya JDP, Barucci MA, Fornasier S, et al (2016) Spectrophotometry of the Khonsu region on the comet 67P/Churyumov–Gerasimenko using OSIRIS instrument images. Monthly Notices of the Royal Astronomical Society 462(Suppl 1):S274–S286. https://doi.org/10.1093/mnras/stw2530

El-Maarry MR, Driver G (2019) Cliff Collapses on Comet 67P/Churyumov-Gerasimenko Following Outbursts as Observed by the Rosetta Mission 2019:EPSC–DPS2019–1727. Conference Name: EPSC-DPS Joint Meeting 2019 ADS Bibcode: 2019EPSC...13.1727R

El-Maarry MR, Groussin O, Thomas N, et al (2017) Surface changes on comet 67P/Churyumov-Gerasimenko suggest a more active past. Science 355(6332):1392–1395. https://doi.org/10.1126/science.aak9384

Fornasier S, Feller C, Lee JC, et al (2017) The highly active Anhur–Bes regions in the 67P/Churyumov–Gerasimenko comet: results from OSIRIS/ROSETTA observations. Monthly Notices of the Royal Astronomical Society 469(Suppl_2):S93–S107. https://doi.org/10.1093/mnras/stx1275

Fornasier S, Feller C, Hasselmann, P. H., et al (2019) Surface evolution of the anhur region on comet 67p/churyumov-gerasimenko from high-resolution osiris images. AA 630:A13. https://doi.org/10.1051/0004-6361/201834824

Hasselmann PH, Barucci MA, Fornasier S, et al (2019) Pronounced morphological changes in a southern active zone on comet 67P/Churyumov-Gerasimenko. Astronomy & Astrophysics 630:A8. https://doi.org/10.1051/0004-6361/201833940

Jindal AS, Birch SPD, Hayes AG, et al (2022) Topographically Influenced Evolution of Large-scale Changes in Comet 67P/Churyumov–Gerasimenko's Imhotep Region. The Planetary Science Journal 3(8):193. https://doi.org/10.3847/PSJ/ac7e48

Knollenberg J, Lin ZY, Hviid SF, et al (2016) A mini outburst from the nightside of comet 67P/Churyumov-Gerasimenko observed by the OSIRIS camera on Rosetta. Astronomy & Astrophysics 596:A89. https://doi.org/10.1051/0004-6361/201527744

Müller DR, Altwegg K, Berthelier JJ, et al (2024) Deciphering cometary outbursts: linking gas composition changes to trigger mechanisms. Monthly Notices of the Royal Astronomical Society 529(3):2763–2776. https://doi.org/10.1093/mnras/stae622

Noonan JW, Rinaldi G, Feldman PD, et al (2021) Analysis of Hybrid Gas–Dust Outbursts Observed at 67P/Churyumov–Gerasimenko. The Astronomical Journal

162(1):4. https://doi.org/10.3847/1538-3881/abf8b4

Pajola M, Höfner S, Vincent JB, et al (2017) The pristine interior of comet 67P revealed by the combined Aswan outburst and cliff collapse. Nature Astronomy 1(5):0092. https://doi.org/10.1038/s41550-017-0092

Preusker F, Scholten F, Matz KD, et al (2017) The global meter-level shape model of comet 67P/Churyumov-Gerasimenko. Astronomy & Astrophysics 607:L1. https://doi.org/10.1051/0004-6361/201731798

Rinaldi G, Bockelée-Morvan D, Ciarniello M, et al (2018) Summer outbursts in the coma of comet 67P/Churyumov–Gerasimenko as observed by Rosetta–VIRTIS. Monthly Notices of the Royal Astronomical Society 481(1):1235–1250. https://doi.org/10.1093/mnras/sty2266

Tang X, Shi X, El-Maarry MR (2025) Boulder Migration in the Khonsu Region of Comet 67P/Churyumov–Gerasimenko. The Astrophysical Journal 979(1):91. https://doi.org/10.3847/1538-4357/ad9825

Vincent JB, A'Hearn MF, Lin ZY, et al (2016) Summer fireworks on comet 67P. Monthly Notices of the Royal Astronomical Society 462(Suppl 1):S184–S194. https://doi.org/10.1093/mnras/stw2409